Transaction F: Nanotechnology
Vol. 17, No. 2, pp. 90–101

Invited Paper

SCIENTIA IRANICA

Mechanical Property Evaluation of Carbon Nanotube Sheets

N. Nouri[1] **and S. Ziaei-Rad**[1,*]

Abstract. *The uses of carbon nanotubes (CNTs) in nanotechnology and leading industries are of extreme importance and they have many applications. One such application is producing nanotube thin pages called buckypaper. These pages, known as nanotube sheets, have significant physical, chemical, mechanical, thermodynamic and electromagnetic properties, such as being several times stronger than steel. In spite of efforts devoted to the development of procedures for the production of buckypaper, not many attempts have been made to understand their mechanical behavior. Computer simulations can be used as a powerful tool to discover the mechanical properties of these materials. The aim of the present research is to investigate the mechanical behavior of buckypaper using the finite element method. Toward this goal, the molecular network of buckypaper, which consists of a regular arrangement of CNTs, is modeled as a structure with its atoms as nodes, its bonds as 3-D-beam elements and Van der Waals forces by means of nonlinear forces. A computer program is then developed to calculate the mechanical properties of buckypaper especially the modulus of elasticity. In this program, the nanotubes are arranged together to create a simple ordered network with periodic boundary conditions resembling real buckypaper. The obtained results from this procedure are compared with those derived from molecular mechanics.*

Keywords: *Buckypaper; Finite element; Mechanical properties; Molecular mechanics; Carbon nanotube sheets.*

INTRODUCTION

Carbon nanotubes (CNTs) have gained significant importance due to their unique mechanical, thermal and electrical properties [1]. There are two main types of carbon nanotube: multi-wall (MWCNTs) and single wall (SWCNTs). Multi-walled carbon nanotubes, as reported in Iijima's nature paper [2], consist of up to several tens of graphite shell, which are in a co-axial seamless, quasi-one-dimensional cylindrical shape, with an adjacent shell separation of approximately 0.34 nanometers (nm). Single wall carbon nanotubes which were first synthesized independently by Iijima and Ichihashi [3] and Bethune et al. [4] in 1993 consist of a single graphite sheet seamlessly wrapped into a cylindrical tube with a diameter of about 1.4 nm, while the length can be up to several millimeters. The carbon atoms in nanotubes are bound together by sp^2 bonds which are much stronger than the sp^3 bonds in a diamond and which provide unusually high strength. Carbon nanotubes are one of the strongest materials ever made known to man; a multi-walled carbon nanotube may have a tensile strength of 63 GPa [5], while that of high-carbon steel is approximately 1.2 GPa. The Young's modulus of nanotubes may reach 1TPa [1], which is several times greater than that of diamonds. Carbon nanotubes also have excellent electrical and thermal properties. Metallic nanotubes can have an electrical current density more than 1,000 times greater than metal, such as silver and copper. Carbon nanotubes have very good thermal conductivity along the tube, which is up to 6000 W/mK at room temperature. It is estimated that carbon nanotubes can keep structural and physical stability up to 2800°C in a vacuum and about 750°C in air [6].

One of the broad applications of CNT is using them for making future nanocomposites because they

1. *Department of Mechanical Engineering, Isfahan University of Technology, Isfahan, P.O. Box 84156-83111, Iran.*
*. *Corresponding author. E-mail: szrad@cc.iut.ac.ir*

Received 10 May 2010; received in revised form 3 October 2010; accepted 2 November 2010

are considered to have specifications like nanotubes. For this purpose, they use arrays of CNTs called buckypaper, which is produced by the vacuum filtration of a nanotube and a water solution, which are then dispersed into resin. Due to the wide range of buckypaper application in industry, knowing its properties is an important task. However, because of the expensive production procedure of nanosheets, the understanding of their nanomechanical behavior is still in its infancy. This shows the importance of developing new methods that are faster and simpler than before, in order to calculate the mechanical properties of this material, using numerical techniques.

In 2002, Terrones and his colleagues investigate molecular junctions between SWCNTs using electron beam welding. In their work, they used electron beam exposure at high temperatures to induce structural defects on SWCNTs and, by this method, promoted the joining capability of the nanotubes for making nanotube sheets [7]. Jiang and Fan [8] were among the first to develop a neat CNT yarn by dry spinning super-aligned arrays of carbon nanotubes. This technique helped to transfer the outstanding properties of CNTs into macroscopic samples. The tensile strength and Young's modulus of these neat CNT fibers were about 600 MPa and 74 GPa, respectively [9]. Zhu and his co-workers [10] directly synthesized SWNT fibers with a tensile strength of 1.2 GPa and Young's modulus of 77 GPa, respectively. In 2003, Coleman et al. investigated the effects of adding polymeric adhesives to the properties of nanotube sheets. By tensile tests on the intercalated sheets, they showed that the Young's modulus, strength and toughness can be increased by factors 3, 9 and 28, respectively. The adding of adhesives resulted in enhancements of intercalated polymers and thus improved the load transmission between nanotubes [11].

Knapp and Schleussner has shown that carbon buckypapers can be used as a large array of electron field emitters for cold cathode applications [12]. Skakalova et al. investigated the effects of gamma irradiation on the Young's modulus and electrical conductivity of the papers made of SWCNTs. Their studies were conducted for irradiation in air or in a vacuum [13]. In 2004, Dharap et al. found that nanotube sheets change their electric properties almost linearly when subjected to mechanical strains. The results indicated that the sheets can be used as a potential material for strain sensing [14]. Zhang and his co-workers presented an oxidization method with nitric acid, which could enhance the tensile modulus and the strength of the buckypaper to about 5 GPa and 75 MPa, respectively. The proposed method, however, decreased the nanotube electrical conductivity [15].

Berhan et al. simulated the network of nanotube ropes with special emphasis on the effect of joint morphology using FEM. They constructed a detailed 3-D model of nanotube joints and tried to model them by an equivalent torsion spring. They then used the equivalent torsion springs for modeling interactions between the nanotubes, which were modeled as 2-D Eulerian beams. Their calculations show a Young's modulus ranging from 15 GPa to 80 GPa, depending on the alignment of the CNTs in the paper [16].

Zhang et al. [17] introduced a dry stretching and twisting process for spinning CNT fibers, resulting in a tensile strength of 460 MPa and an electrical conductivity of 300 S cm^{-1} at room temperature. Ericson, Smalley and co-workers [18] used a conventional spinning method to produce well-aligned SWCNT fibers with a higher Young's modulus of 130 GPa and a tensile strength of 126 MPa. The electrical conductivity of these fibers was 5000 S cm^{-1}, with a thermal conductivity of 21 W $m^{-1}{}^{\circ}K^{-1}$. Li et al. [19] spun CNT fibers directly from the CVD synthesis zone of a furnace. The best electrical conductivity of their CNT fibers was 8 300 S cm^{-1}, and the highest tensile strength reached 1.0 GPa. In 2006, Kulesza et al. showed that the high temperature electrical transport properties of buckypaper composed of doped SWCNT's are nearly temperature independent [20]. Koziol and co-workers [21] combined direct spinning with a post-processing method to obtain high performance CNT fibers. The optimum highest tensile strength of their CNT fiber was 8.8 GPa, and the Young's modulus was 357 GPa. The strength exceeded the mechanical properties of high strength carbon-fiber materials, such as the T1000G carbon fiber from Toray, with a tensile strength of 6.37 GPa [22]. The results prove the potential of using nanotubes for producing a high-performance composite.

MODELING

In this research, two models were used for estimating the modulus of elasticity in the network of nanotubes. The results are then compared and some conclusions will be drawn.

Finite Element Method Model

In this method, molecular networks of buckypaper which consist of an ordered arrangement of nanotubes are modeled as a structure with its atoms as nodes, its bonds as 3-D-elastic-beam elements and Van der Waals forces by means of nonlinear forces.

Constants of the beam elements are calculated by equating the simple harmonic potential and the beam element potential energy, which is graphically shown in Figure 1.

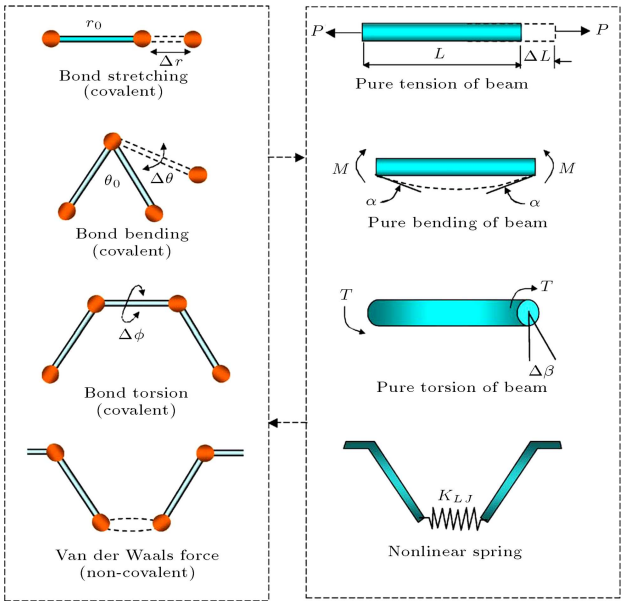

Figure 1. Schematic of bond potential with equivalent element [22].

The formulas below show the beam constants:

$$\left.\begin{aligned}
\Lambda_P &= \int_0^L \frac{P^2}{2AE}dL = \frac{EA}{2L}(\Delta L)^2 = \frac{1}{2}K_r\Delta L^2 \\
\Lambda_M &= \int_0^L \frac{M^2}{2EI}dL = \frac{EI}{2L}(2\alpha)^2 = \frac{1}{2}K_\theta\alpha^2 \\
\Lambda_T &= \int_0^L \frac{T^2}{2GJ}dL = \frac{GJ}{2L}(\Delta\beta)^2 = \frac{1}{2}K_\phi\Delta\beta^2
\end{aligned}\right\} \rightarrow$$

$$\left.\begin{aligned}
\frac{EA}{L} &= K_r \\
\frac{EI}{L} &= k_\theta \\
\frac{GJ}{L} &= K_\phi
\end{aligned}\right\} \Rightarrow \left\{\begin{aligned}
d_b &= \sqrt[4]{\left(\frac{K_\theta}{K_r}\right)} \\
E &= \frac{K_r^2 L}{4\pi K_\theta^2} \\
G &= \frac{K_r^2 L K_\phi}{8\pi K_\theta^2}
\end{aligned}\right. \quad (1)$$

in which d_b stands for the diameter of the beam and E and G are the equivalent Young's and Shear modulus of the beam, respectively. The harmonic bond potential parameters (K_r, K_θ, K_ϕ, L) are extracted from the experimental results of [23-26].

$$\left.\begin{aligned}
\frac{K_r}{2} &= 469\ \frac{\text{kcal}}{\text{mol.A}^{\circ 2}} \\
\frac{K_\theta}{2} &= 63\ \frac{\text{kcal}}{\text{mol.rad}^2} \\
\frac{K_\phi}{2} &= 20\ \frac{\text{kcal}}{\text{mol.rad}^2}
\end{aligned}\right\} \rightarrow \left\{\begin{aligned}
E &= 5.488e-8\ \frac{\text{N}}{\text{A}^{\circ 2}} \\
G &= 8.701e-9\ \frac{\text{N}}{\text{A}^{\circ 2}} \\
d_b &= 1.466\text{A}^\circ
\end{aligned}\right. \quad (2)$$

The extracted constants are used in the following 3-D beam stiffness matrix equation:

$$K^{\text{Local}} = \begin{bmatrix}
AS & 0 & 0 & 0 & 0 & 0 \\
0 & a_z & 0 & 0 & 0 & b_z \\
0 & 0 & a_y & 0 & -b_y & 0 \\
0 & 0 & 0 & TS & 0 & 0 \\
0 & 0 & -b_y & 0 & c_y & 0 \\
0 & b_z & 0 & 0 & 0 & c_z \\
-AS & 0 & 0 & 0 & 0 & 0 \\
0 & -a_z & 0 & 0 & 0 & -b_z \\
0 & 0 & -a_y & 0 & b_y & 0 \\
0 & 0 & 0 & -TS & 0 & 0 \\
0 & 0 & -b_y & 0 & d_y & 0 \\
0 & b_z & 0 & 0 & 0 & d_z
\end{bmatrix}$$

$$\begin{bmatrix}
-AS & 0 & 0 & 0 & 0 & 0 \\
0 & -a_z & 0 & 0 & 0 & b_z \\
0 & 0 & -a_y & 0 & -b_y & 0 \\
0 & 0 & 0 & -TS & 0 & 0 \\
0 & 0 & b_y & 0 & d_y & 0 \\
0 & -b_z & 0 & 0 & 0 & d_z \\
AS & 0 & 0 & 0 & 0 & 0 \\
0 & a_z & 0 & 0 & 0 & -b_z \\
0 & 0 & a_y & 0 & b_y & 0 \\
0 & 0 & 0 & TS & 0 & 0 \\
0 & 0 & b_y & 0 & c_y & 0 \\
0 & -b_z & 0 & 0 & 0 & c_z
\end{bmatrix}, \quad (3)$$

in which the parameters in this matrix are defined in Equation 4. Note that because the bonds are assumed to have a cylindrical shape, I_{zz} is equal to I_{yy}.

$$\left\{\begin{aligned}
&AS = \frac{AE}{L};\ TS = \frac{GJ}{L} \\
&a_z = \frac{12EI_{zz}}{L^3};\ b_z = \frac{6EI_{zz}}{L^2};\ c_z = \frac{4EI_{zz}}{L};\ d_z = \frac{2EI_{zz}}{L} \\
&a_y = \frac{12EI_{yy}}{L^3};\ b_y = \frac{6EI_{yy}}{L^2};\ c_y = \frac{4EI_{yy}}{L};\ d_y = \frac{2EI_{yy}}{L}
\end{aligned}\right. \quad (4)$$

The order of DOFs in the stiffness matrix are u_x^i, u_y^i, u_z^i, θ_x^i, θ_y^i, θ_z^i, u_x^j, u_y^j, u_z^j, θ_x^j, θ_y^j, θ_z^j, respectively. A schematic of the 3-D beam element is shown in Figure 2. Another important point about the beam element is its orientation, which needs to be transferred from the local frame to the global frame. This trans-

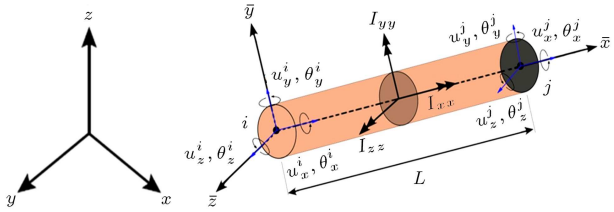

Figure 2. The equivalent 3-D beam element.

formation is carried out using the following equation:

$$K^{\text{Global}} = T^T K^{\text{Local}} T,$$

$$T = \begin{bmatrix} \lambda & 0 & 0 & 0 \\ 0 & \lambda & 0 & 0 \\ 0 & 0 & \lambda & 0 \\ 0 & 0 & 0 & \lambda \end{bmatrix},$$

$$\lambda = \begin{bmatrix} l_1 & m_1 & n_1 \\ l_2 & m_2 & n_2 \\ l_3 & m_3 & n_3 \end{bmatrix}, \quad (5)$$

in which l_i, m_i and n_i are the cosines of the ith local axis of the beam element, with respect to the global frame axis.

For calculating the Van der Waals forces, the following relations (shifted LJ_12_6) were used. In this paper, a cut off distance of about 8.9A° were chosen:

$$\text{SVW}(r) = \begin{cases} W_{LJ}(r) - W_{LJ}(2.5\sigma); & r \le 2.5\sigma \\ 0; & r \ge 2.5\sigma \end{cases} \quad (6)$$

in which W_{LJ} is obeying the following formula:

$$W_{LJ} = 4.\epsilon \left[\left(\frac{\sigma}{r}\right)^{12} + \alpha \left(\frac{\sigma}{r}\right)^{6} \right]. \quad (7)$$

Parameters ϵ, σ and α are 0.03 kcal/mol, 3.8 A° and -1, respectively. From this point, by finding the VDW potential derivative, with respect to the node distances (r), one can have the VDW force as a function of the distance.

$$F_{LJ} = \frac{d(W_{LJ}(r))}{dr} = 4.\frac{\epsilon}{r} \left[-12 \left(\frac{\sigma}{r}\right)^{12} + 6 \left(\frac{\sigma}{r}\right)^{6} \right]. \quad (8)$$

A computer program is developed in MATLAB to create the input for the FE model and also to perform the post-processing of the results. The program has the ability to create nanotube structures with different chiralities. Then it arranges the nanotubes together to create a simple ordered network with periodic boundary conditions, which resembles well real buckypaper. Finally, the reaction forces of the model are calculated and based on the results, the Young's modulus of the system was estimated. A schematic of the FEM model is shown in Figure 3. The nanotube atoms are fixed where they have cut cell boundaries. The main idea in this model is to calculate the highest value that one can obtain from the SWCNT sheet with an ideal nanotube arrangement. Therefore, the results can be considered as an upper limit to the Young's modulus higher than current experimental results. However, it will be shown in the following sections that the results are in agreement with some theoretical predictions reported in [26,27].

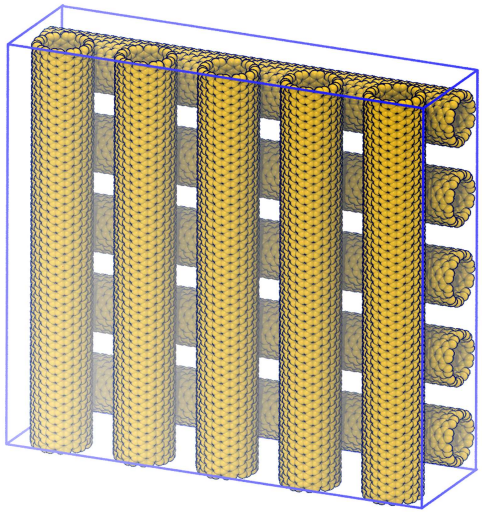

Figure 3. The molecular model of single layer buckypaper and its periodic cell.

Molecular Mechanics Model

Another method for extracting the system behavior is using Molecular Mechanics (MM). Among the different proposed MM methods, here we discuss only some of them, including the method used in this paper. The main idea of using the molecular mechanics method is to benchmark the FEM results from the viewpoint of accuracy and speed.

Stress and Strain in Molecular Scale

Every object or element thereof, which is acted on by external forces, is in a state of stress. Moreover, if the body is in equilibrium, the external stress must be exactly balanced by internal forces. In general, stress is a second rank tensor with nine components, as follows:

$$\begin{bmatrix} \sigma_{11} & \sigma_{12} & \sigma_{13} \\ \sigma_{21} & \sigma_{22} & \sigma_{23} \\ \sigma_{31} & \sigma_{32} & \sigma_{33} \end{bmatrix}. \quad (9)$$

In an atomistic calculation, the internal stress tensor can be obtained using the so-called Virial expression [28]:

$$\sigma = -\frac{1}{V_0} \left[\left(\sum_{i=1}^{N} m_i (v_i v_i^T) \right) + \left(\sum_{i<j} r_{ij} f_{ij}^T \right) \right], \quad (10)$$

where index i runs over all particles from 1 through N; m_i, v_i and f_i denote the mass, velocity and force acting on particle i; and V_0 denotes the (undeformed) system volume. In a static model, the stress tensor is as given in Equation 10 by omitting the first term on the right hand. The application of stress to a body results in a change in the relative position of particles within the

body, expressed quantitatively via the strain tensor:

$$\begin{bmatrix} \epsilon_{11} & \epsilon_{12} & \epsilon_{13} \\ \epsilon_{21} & \epsilon_{22} & \epsilon_{23} \\ \epsilon_{31} & \epsilon_{32} & \epsilon_{33} \end{bmatrix}. \tag{11}$$

For parallelepiped (for example, a periodic simulation cell) characterized in some reference states by three column vectors, $\mathbf{a}_0$, $\mathbf{b}_0$, $\mathbf{c}_0$, and by vectors $\mathbf{a}$, $\mathbf{b}$, $\mathbf{c}$ in the deformed state, the strain tensor is given by:

$$\epsilon = \frac{1}{2}\left[(h_0^T)^{-1} G h_0^{-1} - 1\right], \tag{12}$$

where h_0 denotes the matrix formed from the three column vectors, $\mathbf{a}_0$, $\mathbf{b}_0$, $\mathbf{c}_0$ and h denotes the corresponding matrix formed from $\mathbf{a}$, $\mathbf{b}$ and $\mathbf{c}$. T denotes the matrix transpose, and G denotes the metric tensor $\mathbf{h}^T h$. The elastic stiffness coefficients relating the various components of stress and strain are defined by:

$$C_{imnk} = -\left.\frac{\partial \sigma_{im}}{\partial \epsilon_{nk}}\right|_{T,\epsilon_{nk}} = \left.\frac{1}{V_0}\frac{\partial^2 A}{\partial \epsilon_{lm}\partial \epsilon_{nk}}\right|_{T,\epsilon_{nk},\epsilon_{lm}}, \tag{13}$$

where A denotes the Helmholtz free energy. In principle, one can define adiabatic coefficients in addition to isothermal ones defined by Equation 13, but we will not expand on this here. For more information, refer to standard texts (e.g. [29]). For small deformations, the relationship between the stresses and strains may be expressed in terms of a generalized Hooke's law:

$$\sigma_{lm} = C_{lmnk}\epsilon_{nk}, \tag{14}$$

or alternatively:

$$\epsilon_{lm} = S_{lmnk}\sigma_{nk}, \tag{15}$$

where S_{lmnk} denotes the compliance components. In view of the fact that both stress and strain tensors are symmetric, it is often convenient to simplify these expressions by making use of the Voigt vector notation. As we know, stress is represented as:

$$\begin{bmatrix} \sigma_{11} & \sigma_{12} & \sigma_{13} \\ \sigma_{21} & \sigma_{22} & \sigma_{23} \\ \sigma_{31} & \sigma_{32} & \sigma_{33} \end{bmatrix} \rightarrow \begin{bmatrix} \sigma_1 & \sigma_6 & \sigma_5 \\ \sigma_6 & \sigma_2 & \sigma_4 \\ \sigma_5 & \sigma_4 & \sigma_3 \end{bmatrix}. \tag{16}$$

For example:

$$\sigma = \begin{bmatrix} \sigma_{11} & \sigma_{22} & \sigma_{33} & \sigma_{23} & \sigma_{13} & \sigma_{12} \end{bmatrix}^T, \tag{17}$$

while strain is represented as:

$$\epsilon = \begin{bmatrix} \epsilon_{11} & \epsilon_{22} & \epsilon_{33} & 2\epsilon_{23} & 2\epsilon_{13} & 2\epsilon_{12} \end{bmatrix}^T. \tag{18}$$

The generalized Hooke's law is thus often written as:

$$\sigma_i = C_{ij}\epsilon_j. \tag{19}$$

Note that 6×6 elastic matrix C is also symmetric and hence a maximum of 21 coefficients are required to describe the stress-strain behavior of an arbitrary material fully. In addition, C is no longer a tensor, since it does not obey the required transformation rules. As an example for the material we have here, the stress-strain behavior can be fully described by specifying only six independent coefficients. The resulting elastic matrix may be written as:

$$[C] = \begin{bmatrix} C_1 & C_3 & C_4 & 0 & 0 & 0 \\ & C_2 & C_3 & 0 & 0 & 0 \\ & & C_1 & 0 & 0 & 0 \\ & & & C_5 & 0 & 0 \\ & \text{Sym} & & & C_6 & 0 \\ & & & & & C_5 \end{bmatrix}. \tag{20}$$

Molecular Mechanic Methods for Extracting Elastic Constants

To date, reported attempts to estimate the elastic moduli of amorphous polymers have adopted one of three approaches. The first approach originating in the work of Theodorou and Suter [30] uses a completely static technique. Briefly, Theodorou and Suter performed a detailed theoretical study of the various factors contributing to the elastic constants, as formally defined by Equation 13. They concluded that the configurational entropy and strain dependency of the vibrational frequencies are negligible for glassy propylene. Consequently, it should be possible to estimate the elastic stiffness coefficients from numerical estimates of:

$$\frac{d^2U}{d\epsilon_i d\epsilon_j} = \frac{d\sigma_i}{d\epsilon_j}. \tag{21}$$

Thus, having constructed an energy-minimized series of amorphous structures confined to a periodic cube, each structure is subjected to twelve deformations; three pairs in uniaxial tension/compression and three pairs involving pure shear, followed by a reminimization to restore a state of detailed mechanical equilibrium. Each of these deformations corresponds to setting one of the components of the strain tensor (Equation 11) to some small value (for example $\varepsilon = 0.001$), while keeping all other components fixed at zero. The elastic stiffness coefficients can then be obtained by estimating the second derivatives of the deformation energy, with respect to strain, using a finite difference formula (for the diagonal components only), and by calculating $\Delta\sigma_i/\Delta\varepsilon_j$ for each of the six pairs of applied strains where σ_i represents, in vector notation, elements of the stress tensor obtained analytically using the Virial Equation 10. Although both of these methods gave good agreement for the diagonal elements, C_{ii}, of the stiffness matrix for the glassy polypropylene samples studied in [30], generally, it should be assumed that numerical estimation of second derivatives (of the

energy) will be less precise than estimation of the first derivatives (of the stress). Therefore, the latter method is preferred.

A second approach for obtaining the elastic modulus involves using constant stress molecular dynamics to measure the stress-strain behavior of a material subjected to an applied load. This approach has been used to investigate the stress-strain behavior and estimate the modulus of samples of amorphous polyethylene modeled using a united-atom approach. In [31], the constant stress dynamics method of [32] was modified to ensure that matrix h, made up from cell vectors **a**, **b** and **c**, remains symmetric during the simulation. The simulation consisted of increasing the magnitude of an applied tensile stress at a constant rate of either 1 bar/ps or 5 bar/ps. The resulting longitudinal and average lateral strain were then monitored during the simulation and used to estimate Young's modulus, Poisson's ratio and the yielding behavior of the material at various temperatures. It should also be noted that the approach used in [32], which does not correspond to any of the ensembles encountered in statistical thermodynamics, was chosen in preference to the theoretically more rigorous approach presented in [33], which generates the constant stress ensemble, because it is relatively free from the unphysical oscillatory fluctuations of the cell. These arise because the difference between internal stress and applied stress is coupled to the first derivative of the cell vectors, with respect to time, rather than to the second derivative.

One potential advantage of the dynamics approach, over the static method described above, is that the entropic effects ignored by the latter are implicitly included. Moreover, the dynamics approach in principle allows study of yielding, albeit under conditions of an extremely rapid rate of application of stress. However, using molecular dynamics has a number of significant disadvantages. Firstly, it typically requires long duration simulations (Brown and Clarke [31] used O (10^6) integration steps per stress-strain experiment, consisting of the application of stress in a single direction). Secondly, the strain fluctuates with time, even when the system is subjected to a non time-dependent stress. Consequently, there are uncertainties in its measurement. These are further amplified in a dynamical experiment in which the stress is increased at a constant rate. We might attempt to eliminate this artifact by increasing the stress stepwise, waiting until the strain equilibrates before incrementing the stress. However, polymer experimentalists will be familiar with the fact that the strain may increase on the time scale of seconds to days after application of a stress.

The third class of method for obtaining stiffness coefficients, which also implicitly captures entropic effects, uses fluctuation formulas applied to simulations in different ensembles. The simplest formula applicable when simulations have been performed in the constant stress ensemble is as follows [34]:

$$C_{ik} = \frac{kT}{\langle V \rangle} \langle \epsilon_i \epsilon_j \rangle^{-1}. \tag{22}$$

In practical applications, convergence of this expression tends to be relatively slow, typically requiring simulations containing a minimum of 10^5 samples to obtain reasonably precise estimates (for example within 10% of the values obtained from fully converged runs). As pointed out by [35], alternative fluctuation formulas exist for ensembles, in which the shape of the simulation cell is held fixed. While these methods do show improved convergence behavior, the formulas are more difficult to apply in practice, due to the presence of terms that depends on the second derivatives of energy, with respect to atomic positions. More recently, an alternative fluctuation expression has been presented by [36], which gives a good approximation by the following relation:

$$C_{ik} = \langle \epsilon_i \sigma_j \rangle \langle \epsilon_i \epsilon_j \rangle^{-1}, \tag{23}$$

where the repeated indices imply use of the summation convention. When used to calculate the elastic constants of the nearest neighboring FCC argon crystal between 1 K and 36 K, Equation 16 showed significantly improved convergence behavior over Equation 23.

In conclusion, taking into consideration the general desirability of averaging property measurements for amorphous polymers over as many independent samples as possible, the static and rapidly-converging fluctuation methods probably offer the most desirable approaches available at the present time. Therefore, the first approach is used as the processing method in the paper.

In this model, molecular coordinates of the buckypaper network are exported to the molecular mechanic/dynamic program, and after energy minimization with the conjugate gradient method under periodic boundary conditions, the strain energy of the system is calculated. The application of strain was performed by first uniformly expanding the dimensions of the MM cell in the direction of the deformation, then the new coordinates of the atoms were rescaled to fit within the new dimensions [37]. Next, the MM simulation for this new MM cell was carried out and the atoms were allowed to equilibrate within the new MM cell dimensions. This process was repeated for every increment of the deformation. In each increment, the strain energy was minimized and recorded and then the Young's modulus was calculated from the second derivative of the strain energy density, with respect to

various strains [38,39]:

$$\sigma_{ij} = \frac{1}{V_0}\left(\frac{\partial E}{\partial \epsilon_{ij}}\right), \tag{24}$$

where E is the strain energy and ϵ_{ij} is the strain tensor. It is noteworthy that both FEM and MM techniques have estimated almost the same results of buckypaper behavior for small deformations, when the same potential energy parameters (K_r, K_φ, K_θ) are used for carbon atom interactions.

RESULTS AND DISCUSSIONS

Benchmark

For a single wall CNT with chirality (7,7), diameter 9.5588 and infinite length, the simulation results from both FE and MM predict a Young's modulus between 0.75 TPa to 0.96 TPa, which is lower than the value 0.972 TPa reported by [38], and higher than the results (0.5 $\sim$ 0.6 TPa) from [40]. Table 1 compares the accuracy and speed of calculations between FEM and MM methods for this case study. It is noted from the table that FEM is almost an order of magnitude faster than MM. Meanwhile, one can conclude that the accuracy of both results is almost of the same order.

Single Layer Nanotubes with Infinite Length

A study is carried out with nanotubes continuous along the cell (long fibber), but the estimated modulus being very high (Figure 3). In this model, we assume that there is only one layer of nanotubes and the nanotubes are infinitely long. In the simulation of single layer buckypaper, the separation distance between the crossed CNTs in the radius direction of the model is 3.1A°. The length, width and height of the cell are assumed to be 23.117692, 23.117692, 25.317692A°, respectively. For this case, a Young's modulus of 0.35 TPa for buckypaper was obtained. By increasing the separation distance from 2A° to 7A° between nanotubes in the buckypaper model, the value of the Young's modulus reduced from 0.349 TPa to 0.267 TPa, as shown in Figure 4. This can be explained by the fact that by increasing the nanotube distance, the Van der Waals forces decreases, which, in turn, decreases the interaction force between nanotubes and consequently results in a reduction in the elastic modulus.

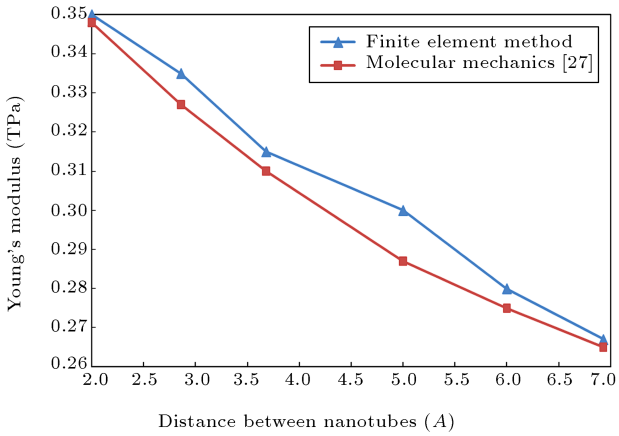

Figure 4. Young's modulus of buckypaper versus distance between parallel nanotubes.

Because of obtaining similar results from both techniques and also due to less computational effort required by the FEM method, it was decided to carry out all calculations by FEM technique only hereafter.

The length of the carbon nanotubes is equal to the unit cell length in simulation of the buckypaper model. Next, different lengths of the unit cell in x and y directions (i.e. 2.35, 4.95, 5.20, 6.09, 7.3 and 9.7 nm) were used to build the one-layer buckypaper model. Then, the FEM simulation was accomplished to investigate the effect of unit cell length on the Young's modulus of buckypapers. It was found that the longer the nanotube length, the lower the buckypaper Young's modulus. Figure 5 shows the variation of Young's modulus for different unit cell lengths. The reason for reduction in the Young's modulus value is that the longer the unit cell, the bigger the distance between the neighboring nanotubes in the buckypaper. In other words, the number of nanotubes is kept constant while the cell sizes are increased, therefore, the distance between nanotubes is increased, which results in a decrease in Van der Waals interaction forces. The results are compared with those calculated by MM and

Table 1. Predicted Young's modulus and CPU time for a SWCNT by FEM and MM approaches.

CNT	FEM (TPa)	MM (TPa)	Experiment (TPa) [41]	CPU Time (Seconds)	
				FEM	MM
Chirality (7,7) l = infinite	0.749 $\sim$ 0.856	0.784 $\sim$ 0.837	0.250 $\sim$ 0.950	1213.2	9473.7
Chirality (5,5) l = infinite	0.876 $\sim$ 0.933	0.891 $\sim$ 0.924		597.9	4768.3

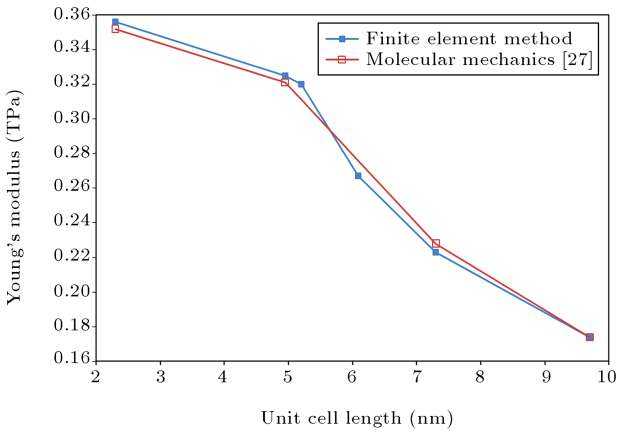

Figure 5. Variation of Young's modulus versus unit cell length in x and y directions.

reported in [27], and show the validity of the proposed technique in this paper.

However, the obtained Young's modulus values for buckypaper were higher than the reported experimental results from [15,16,19,41]. The most important reason for this can be explained by the fact that the simulation model disregarded lots of flaws, such as impurity particles, uneven thickness and misalignments, which can significantly reduce the Young's modulus of buckypaper. However, the most influential parameter is the infinite length that has been assumed for the nanotubes; this value may represent an upper limit for the Young's modulus of buckypaper, as will be addressed in upcoming sections. Recently, in new experimental research depicted in journals of advanced functional materials, the researchers have been able to make buckypaper from very long CNTs (with aspect ratio about 100000), which results in the Young's modulus reaching about 170 GPa [41]. This value for the elastic modulus is in good agreement with the value obtained for the unit cell length 9.8 nm in Figure 5.

Multi Layer Nanotubes with Infinite Length

Next, it was decided to repeat the calculations for a multilayer buckypaper (Figure 6). For this type of buckypaper, the simulation results, together with those obtained from MM simulation, are depicted in Figure 7. The Young's modulus decreases from 0.326 TPa to 0.189 TPa, while the layer number of the buckypaper varies from 1 to 5. This is due to the gap between layers, which reduces system stiffness. It can be found that the Young's modulus converges to a limit of around 0.19 TPa, as shown in Figure 7.

Single Layer Nanotubes with Finite Length

In this model, an effort was made to improve model accuracy and approach experimental values reported

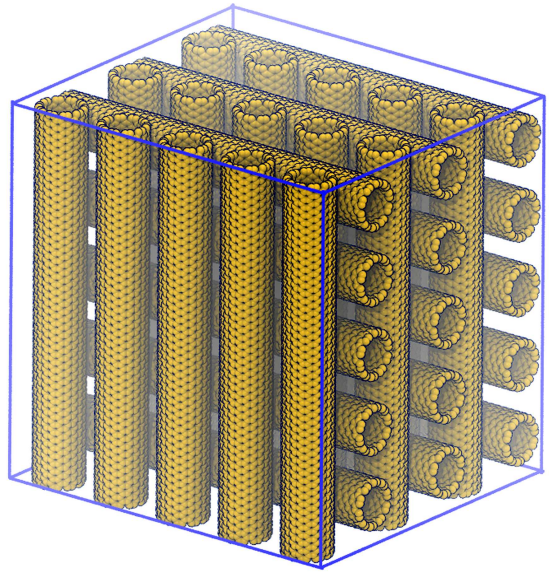

Figure 6. Multilayer buckypaper (three layers).

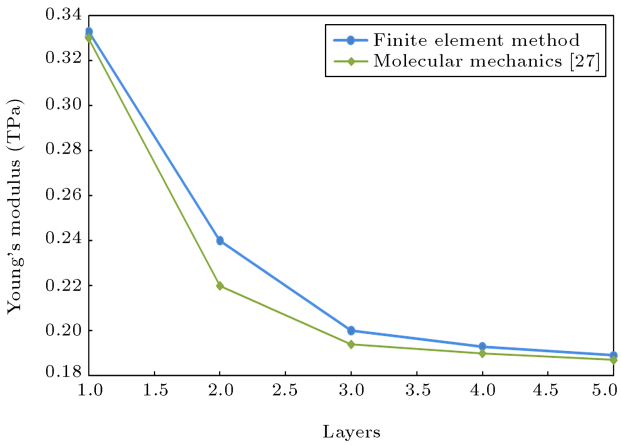

Figure 7. Variation of Young's modulus of buckypaper versus the layer number.

in the literature by changing the nanotube arrangement and boundary conditions. In spite of the first model, the main idea in this model is that the Van der Waals forces are the only reason for keeping the structure strength under various loading conditions. Therefore, nanotube are no longer infinite. However, due to limitations in computational cost, the aspect ratio in this model is lower compared with the real situation. Therefore, the results can be considered as a lower bond to actual material behavior; it is noteworthy that the model has one layer only. The new simulation system and its boundary conditions are shown in Figure 8. In this case, a Young's modulus of 13.57 GPa is obtained for the one layer buckypaper system. By increasing the separation distance between nanotubes from 2A° to 7A°, as before, the value of Young's modulus is reduced, as shown in Figure 9.

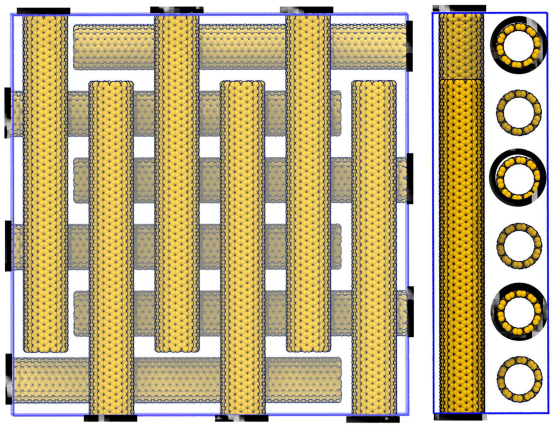

Figure 8. The molecular model of single layer buckypaper (front and side views) and its periodic cell with boundary conditions used in the solution.

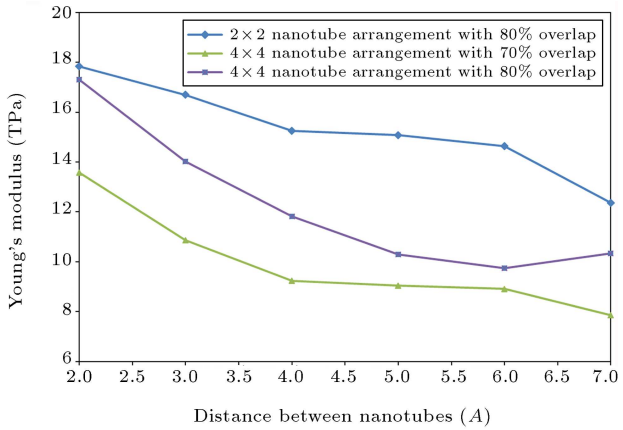

Figure 9. Young's modulus of buckypaper versus distance between parallel nanotubes.

Multi Layer Nanotubes with Finite Length

Next, it was decided to repeat the calculation for multilayer buckypaper, as shown in Figure 10. For multilayer buckypaper, the simulation results are depicted in Figure 11. The Young's modulus decreases from 18 GPa to 9.48 GPa, while the layer number of buckypaper varies from 1 to 5. This is due to the gap between layers, which reduces system stiffness. It can be found that the Young's modulus converges to a limit of around 9 GPa, as shown in Figure 11.

The length of the carbon nanotubes is equal to a portion unit cell length in the simulation of buckypaper. Then, the finite element simulation is carried out to investigate the effect of unit cell length on the Young's modulus of buckypaper. It was found that the longer the cell length, the lower the buckypaper Young's modulus. The results indicate that by increasing overlap between nanotubes, the young modulus increases rapidly. Figure 12 shows the variation of the Young's modulus for different unit cell length. The reason for reduction in the Young's modulus value is

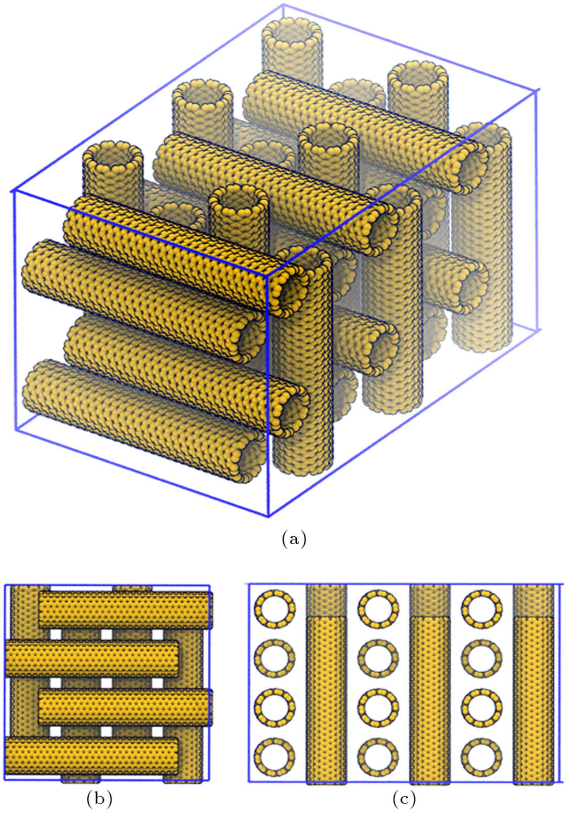

Figure 10. Multilayer (three layer) buckypaper with its periodic cell. (a) Isometric view; (b) front view; and (c) side view.

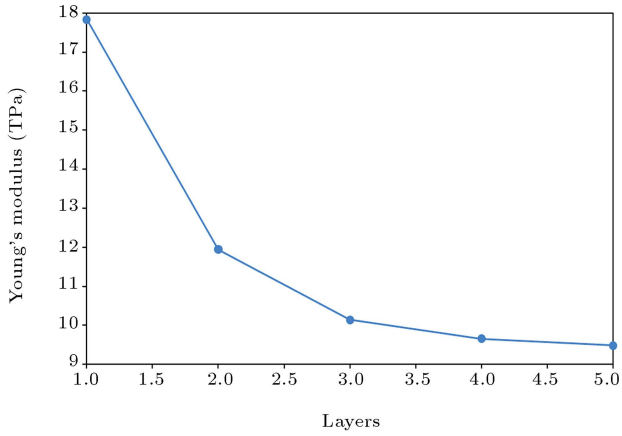

Figure 11. Variation of Young's modulus of buckypaper versus the layer number.

the same as explained for the first model. The obtained Young's modulus values for buckypaper show good agreement with the range of reported experimental and theoretical results, as shown in Table 2.

CONCLUSIONS

The mechanical properties of carbon nanotube sheets, i.e. buckypaper, were studied by finite element analysis

Table 2. Young's modulus of buckypaper (prediction versus experimental).

	Multi-Layer (MM)	**Multi-Layer (FEM)**	**Experimental and Theoretical (GPa)**
Young's Modulus of Buckypaper with Finite Nanotube Length	9.34 GPa	8.76 GPa	[16]: minimum 15 [42]: 8 [43]: 5.04 ∼ 6.06 [44]: 2 ∼ 12 [45]: 45
Young's Modulus of Buckypaper with Infinite Nanotube Length	192 GPa	189 GPa	[16]: max 80 [46]: 169

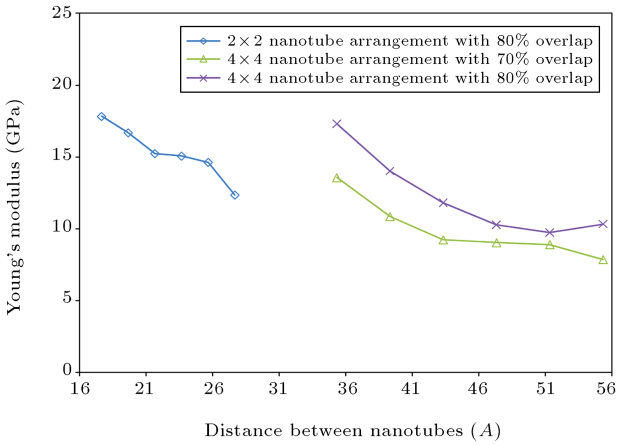

Figure 12. Variation of Young's modulus versus the unit cell length in x and y directions.

and molecular mechanical simulation. The findings indicate that the finite element results are almost as accurate as the molecular mechanical model. It was also found that due to the use of the second derivative of energy in the calculation of strain by MM, the FEM is almost an order of magnitude faster than MM.

For the single wall CNTs, a reasonable Young's modulus, 0.75 ∼ 0.96 TPa was obtained, which is comparable with values reported in other research work. In the simulation of single layer buckypaper with finite CNT length, a Young's Modulus of 13.57 GPa was calculated, while by assuming infinite length, a Young's modulus of 190 GPa is extracted using the FEM approach. This shows that the assumption of finite length is an important hypothesis in the simulation of real buckypaper.

In both finite and infinite length models, by increasing the separation distance between nanotubes in the buckypaper, the value of Young's modulus is reduced. The obtained Young's modulus values for buckypaper have good agreement with available experimental results.

REFERENCES

1. Treacy, M.M.J., Ebbesen, T.W. and Gibson, J.M. "Exceptionally high Young's modulus observed for individual carbon nanotubes", *Nature*, **381**, p. 678 (1996).
2. Iijima, S. "Helical microtubules of graphitic carbon", *Nature*, **354**, pp. 56-68 (1991).
3. Iijima, S. and Ichihashi, T. "Single-shell carbon nanotubes of 1-nm diameter", *Nature*, **363**, pp. 603-605 (1993).
4. Bethune, D.S., Kiang, C.H., de Vries, M.S., Gorman, G., Savoy, R., Vazquez, J. and Beyers, R. "Cobalt-catalysed growth of carbon nanotubes with single-atomic-layer walls", *Nature*, **363**, pp. 605-607 (1993).
5. Yu, M.F. "Strength and breaking mechanism of multiwalled carbon nanotubes under tensile load", *Science*, **287**, pp. 637-640 (2002).
6. Collins, Ph.G. and Avouris, Ph. "Nanotubes for electronics", *Scientific American*, **283**, pp. 62-69 (2000).
7. Terrones, M., Banhart, F., Grobert, N., Charlier, J.-C., Terrones, H. and Ajayan, P.M. "Molecular junctions by joining single-walled carbon nanotubes", *Physical Review Letters*, **89**(7), 075505-4 (2002).
8. Jiang, K., Li, Q. and Fan, S., *Nature*, **419**, p. 801 (2002).
9. Zhang, X.B., Jiang, K.L., Teng, C., Liu, P., Zhang, L., Kong, J., Zhang, T.H., Li, Q.Q. and Fan, S.S., *Adv. Mater.*, **18**, p. 1505 (2006).
10. Zhu, H.W., Xu, C.L., Wu, D.H., Wei, B.Q., Vajtai, R. and Ajayan, P.M., *Science*, **296**, p. 884 (2002).
11. Colemana, J.N., Blau, W.J., Dalton, A.B., Munõz, E., Collins, S., Kim, B.G., Razal, J., Selvidge, M., Vieiro, G. and Baughman, R.H. "Improving the mechanical properties of single-walled carbon nanotube sheets by intercalation of polymeric adhesives", *Applied Physics Letters*, **82**(11), pp. 1682-1684 (2003).
12. Knapp, W. and Schleussner, D. "Carbon buckypaper field emission investigations", *Vacuum*, **69**, pp. 333-338 (2003).

13. Skákalová, V., Hulman, M., Fedorko, P., Luká, P. and Roth, S. "Effect of gamma-irradiation on single-wall carbon nanotube paper", *AIP Conf. Proc.*, **685**, pp. 143-147 (2004).

14. Dharap, P., Li, Z., Nagarajaiah, S. and Barrera, E.V. "Nanotube film based on single-wall carbon nanotubes for strain sensing", *Nanotechnology*, **15**, pp. 379-382 (2004).

15. Zhang, Xi., Sreekumar, T.V., Liu, T. and Kumar, S. "Properties and structure of nitric acid oxidized single wall carbon nanotube films", *J. Phys. Chem. B*, **108**, pp. 16435-16440 (2004).

16. Berhan, L., Yi, Y.B., Sastrya, A.M., Munoz, E., Selvidge, M. and Baughman, R. "Mechanical properties of nanotube sheets: Alterations in joint morphology and achievable moduli in manufacturable materials", *Journal of Applied Physics*, **95**(8), pp. 4335-4345 (2004).

17. Zhang, M., Atkinson, K.R. and Baughman, R.H. "Multifunctional carbon nanotube yarns by downsizing an ancient technology", *Science*, **306**, p. 1358 (2004).

18. Ericson, L.M., Fan, H., Peng, H.V., Davis, A., Zhou, W., Sulpizio, J., Wang, Y., Booker, R., Vavro, J., Guthy, C., Parra-Vasquez, A.N.G., Kim, M.J., Ramesh, S., Saini, R.K., Kittrell, C., Lavin, J.G., Schmidt, H., Adams, W.W., Billups, W.E., Pasquali, M., Hwang, W.-F., Hauge, R.H., Fischer, E. and Smalley, R.E "Macroscopic, neta, single-walled carbon nanotube fibers", *Science*, **305**, p. 1447 (2004).

19. Li, Y.L., Kinloch, I.A. and Windle, A.H. "Direct spinning of carbon nanotube fibers from chemical vapor deposition synthesis", *Science*, **304**, p. 276 (2004).

20. Kulesza, S., Szroeder, P., Patyk, J.K., Szatkowski, J. and Kozanecki, M. "High-temperature electrical transport properties of buckypapers composed of doped single-walled carbon nanotubes", *Carbon*, **44**, pp. 2178-2183 (2006).

21. Koziol, K., Vilatela, J., Moisala, A., Motta, M., Cunniff, P., Sennett, M. and Windle, A. "Carbon nanotube fiber fabrication", *Science*, **318**, p. 1892 (2007).

22. Today Carbon Fibers America, Inc. High Strength Carbon Fibers, http://www. toraycfa.com/pdfs/ T1000GData Sheet.pdf (last accessed February 2009).

23. Allinger, N.L., Yuh, Y.H. and Lii, J.H. "Molecular mechanics: the MM3 force field for hydrocarbons", *Journal of the American Chemical Society*, **111**, pp. 8551-8566 (1989).

24. Cornell, W.D., Cieplak, P. and Bayly, C.I. "A second generation force-field for the simulation of proteins, nucleic-acids, and organicmolecules", *Journal of American Chemical Society*, **117**, pp. 5179-5197 (1995).

25. Jorgensen, W.L. and Severance, D.L. "Aromatic aromatic interactions-free energy profiles for the benzene dimmer in water, chloroform, and liquid benzene", *Journal of American Chemical Society*, **112**, pp. 4768-4774 (1990).

26. Kalamkarov, A.L., Georgiades, A.V., Rokkam, S.K., Veedu, V.P. and Ghasemi-Nejhad, M.N. "Analytical and numerical techniques to predict carbon nanotubes properties", *International Journal of Solids and Structures*, **43**, pp. 6832-6855 (2000).

27. Ji, Y. "Multiscale investigations on structural properties and mechanical applications of carbon nanotube sheets", PhD Thesis, The University of Akron, USA, (2007).

28. Accelrys Material Studio 5.0 Documentation, Accelrys Software Inc.

29. Weiner, J.H., *Statistical Mechanics of Elasticity*, John Wiley, New York (1983).

30. Theodorou, D.N. and Suter, U.W. "Atomistic modeling of mechanical properties of polymeric glasses", *Macromolecules*, **19**, pp. 139 (1986).

31. Brown, D. and Clarke, J.H.R. "Molecular dynamics simulation of an amorphous polymer under tension. 1. Phenomenology", *Macromolecules*, **24**, pp. 2075 (1991).

32. Berendsen, H.J.C., Postma, J.P.M., van Gunsteren, W.F., DiNola, A. and Haak, J.R. "Molecular dynamics with coupling to an external bath", *J. Chem. Phys.*, **81**, pp. 3684-3690 (1984).

33. Parrinello, M. and Rahman, A. "Polymorphic transitions in alkali halides, a molecular dynamics study", *J. Phys.*, Paris, C6, p. 511 (1981).

34. Parrinello, M. and Rahman, A. "Strain fluctuations and elastic constants", *J. Chem. Phys.*, **76**, p. 2662 (1982).

35. Ray, J.R. "Elastic constants and statistical ensembles in molecular dynamics", *Comput. Phys. Rep.*, **8**, pp. 109 (1988) and references therein.

36. Gusev, A.A., Zehnder, M.M. and Suter, U.W. "Fluctuation formula for elastic constants", *Phys. Rev. Rep. B*, **541** , 06726-4 (1996).

37. Frankland, S.J.V., Harik, V.M., Odegard, G.M., Brenner, D.W. and Gates, T.S. "The stress-strain behavior of polymer-nanotubes composites from molecular dynamics simulation", *Composites Science and Technology*, **63**, pp. 1665-1661 (2003).

38. Lu, J.P. "Elastic properties of carbon nanotubes and nanoropes", *Physics Review Letters*, **79**, pp. 1297-1300 (1997).

39. Huntington, J.B., *Solid State Physics*, Seitz, F. and Turnbull, D., Eds., **7**, p. 16, Academic, New York, USA (1958).

40. Pipesa, R.B., Franklandb, S.J.V., Hubertc, P. and Saether, E. "Self-consistent properties of carbon nanotubes and hexagonal arrays as composite reinforcements", *Composites Science and Technology*, **63**, pp. 1349-1358 (2003).

41. Salvetat, J.P., Briggs, G.A.D., Bonard, J.M., Bacsa, R.R., Kulik, A.J., Stöckli, T., Burnham, N.A. and Forró, L. "Elastic and shear moduli of single-walled carbon nanotube ropes", *Physical Review Letters*, **82**, pp. 944-947 (1999).

42. Sreekumar, T.V., Liu, T., Kumar, S., Ericson, L.M., Hauge, R.H. and Smalley, R.E. "Single-wall carbon nanotube films", *Chemistry of Materials*, **15**(1), pp. 175-178 (2003).

43. Brayford, P.A. "Mechanical properties of buckypaper laminate composites and buckypaper subjected to microwave irradiation", *Colorado School of Mines*, **19**(18), pp. 1-20 (2008).

44. Zaeri, M.M., Ziaei-Rad, S. and Vahedi, A. "The mechanical modeling of carbon nanomaterials from nanotubes to buckypaper", *Carbon*, **48**, pp. 3916-3930 (2010).

45. Wang, B., Shankar, R., Liang, Zh., Wang, Zh., Zhang, C. and Kramer, L. "Theoretical prediction and experimental study of mechanical properties for random and magnetically aligned single-walled carbon nanotube/epoxy composites", *Material Research Society, Proceedings of Materials Research Society Symposium, Symposium Q10.1, Mechanical Properties of Nanostructured Materials and Nanocomposites*, Boston, MA, USA (2003).

46. Cheng, Q., Bao, J., Park, J.G., Liang, Zh., Zhang, Ch. and Wang, B. "High mechanical performance composite conductor: Multi-walled carbon nanotube sheet/bismaleimide nanocomposites", *Advanced Functional Materials*, **19**, pp. 2119-3225 (2009).

BIOGRAPHIES

Nima Nouri received both his B.S. and M.S. degrees in Mechanical Engineering from Isfahan University of Technology, Iran, in 2009 and 2010, respectively. He is now a Ph.D. student at the same university in the Department of Mechanical Engineering; his research being in the field of Applied Mechanics.

Saeed Ziaei-Rad received both his B.S. and M.S. degrees in Mechanical Engineering from Isfahan University of Technology, Iran, in 1988 and 1990, respectively. He obtained his Ph.D. degree from the Department of Mechanical Engineering at Imperial College of Science and Technology, UK, in 1997. He is an Academic Member of the Mechanical Engineering Department of Isfahan University of Technology and has published many papers in international journals and at conferences.